Zhang et al. *NPG Asia Materials* (2023) 15:44
https://doi.org/10.1038/s41427-023-00490-z

NPG Asia Materials

ARTICLE Open Access

Viscoelastic, ductile and repairable carbon nanotube films formed with CNT/PEI double networks containing branched polyethylenimine

Xiaohua Zhang[1], Xin Wang[1], Xin Zhang[2], Jingyun Zou[2,3], Yongyi Zhang[2,4], Jingna Zhao[2,4] and Qingwen Li[2]

Abstract

Manipulating nanostructure assemblies is important in using them as structural and functional materials. Carbon nanotubes (CNTs) lack the ability to reconstruct their entangled network. In this work, we report a strategy with which to realize efficient manipulation of CNT networks by forming double networks with branched polyethylenimine (PEI). The double network was highly viscoelastic and ductile and enabled efficient film stretching or creeping for CNT alignment, which dramatically improved the mechanical strength of the CNT films. Due to the viscous drag from the polymer network, the CNTs showed enhanced movability in reconstructing new networks, which made the film repairable. The repairability resulted from the branched polymeric structure. This double-networking strategy provides a new way to manipulate CNT assemblies for high-performance applications.

Introduction

The story of human civilization can be read in the materials we have found, created, used, and abused. These materials have evolved from natural materials of bone, wood, and shells, in the early stages to today's synthetic compounds that offer much improved performances. Researchers have focused on the distinctive qualities of the elegant and complex architectures of biomaterials (or bio-composites), which have shown many advantages, including biocompatibility, biodegradability, remodeling, self-healing, lightweight, and superior mechanical properties[1–4]. To develop additional multifunctional composites that mimic biomaterials, carbon nanotubes (CNTs) have been composited with polymers. The CNTs act as the major components (bricks) to carry the external stresses and the polymer matrix acts as interfacial adhesives (mortars) to combine the CNTs together, to form a brick-and-mortar or hierarchical multiscale structure[5–10]. To realize such composition, one should introduce polymer into CNT scaffolds or networks via various infiltration/impregnation methods, while the vice versa dispersion of CNTs into the polymer matrix (e.g., melts and solutions) is not applicable. Macroscopic CNT assemblies have become the best choice as the bricks[8,9,11–14], and the chemical vapor deposited (CVD) CNT films[15–17] are suitable owing to the dense CNT connections (or joints).

Unfortunately, since CNTs are not as processable as polymers, it is very challenging to directly realize the optimal composite structure or to efficiently optimize the structure with various post-treatments[8]. For high-performance CNT/polymer composites with a high CNT mass fraction (at least >50%), the following issues should be considered: (1) high overall packing density, (2) highly ordered CNT distribution, (3) reduced CNT aggregation (to utilize all CNT surfaces), and (4) efficient interfacial stress transfer[8,18,19]. However, present manipulation

Correspondence: Xiaohua Zhang (zhangxh@dhu.edu.cn) or
Jingyun Zou (jyzou2021@usts.edu.cn) or
Jingna Zhao (jnzhao2008@sinano.ac.cn)
[1]Innovation Center for Textile Science and Technology, College of Textiles, and MOE Key Laboratory of Textile Science & Technology, Donghua University, Shanghai 201620, China
[2]Advanced Materials Division, and Key Laboratory of Multifunctional Nanomaterials and Smart Systems, Suzhou Institute of Nano-Tech and Nano-Bionics, Chinese Academy of Sciences, Suzhou 215123, China
Full list of author information is available at the end of the article

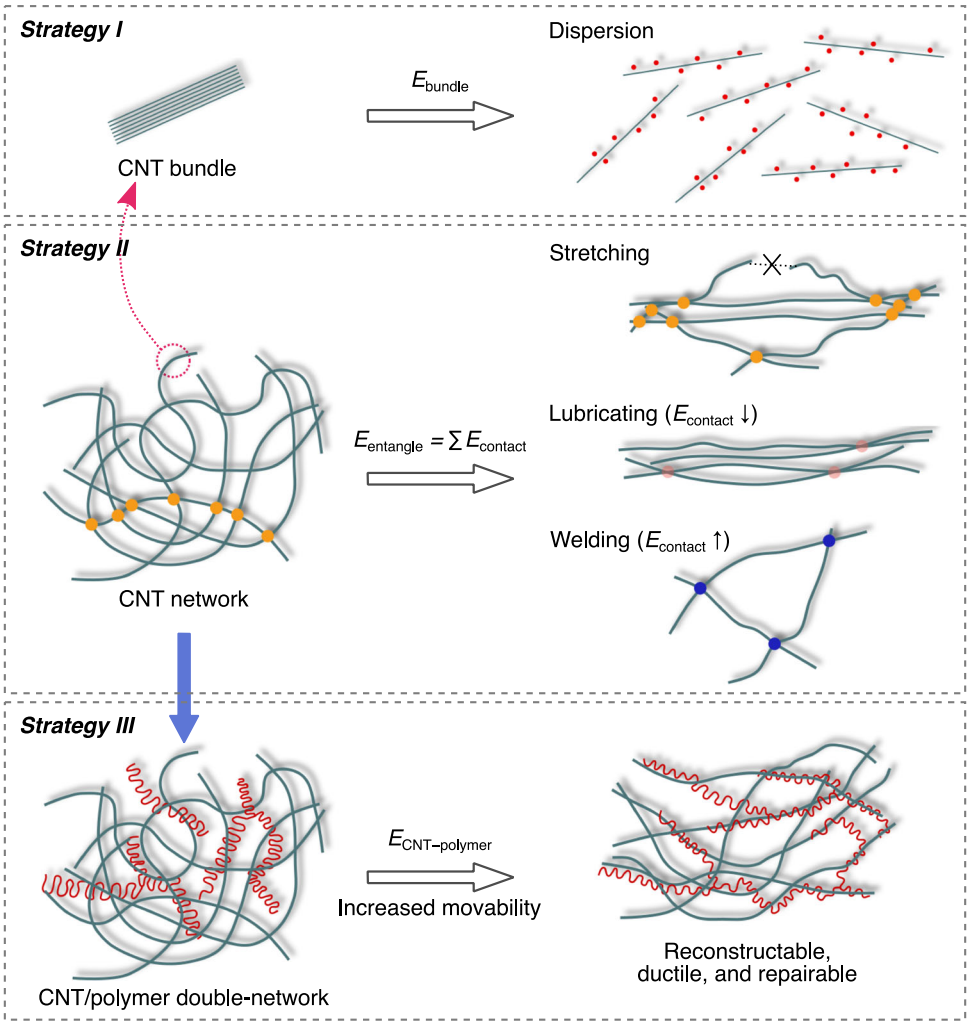

Fig. 1 Schematics to show the processing strategies of CNTs. The first strategy is based on the CNT dispersion where the bundling energy (E_{bundle}) should be overcome. The second one is to directly manipulate CNT network by dealing with the entanglement energy ($E_{entangle}$)– a sum of the contact energy between CNTs ($E_{contact}$). The third one will introduce branched polymers into the CNT networks. The inter-network interaction (*E*CNT–polymer) will lead to various advantages concerning with the increased CNT movability in the formed CNT/polymer double network.

methods can hardly realize these purposes at once due to their limited capacity to reassemble CNT networks. Figure 1 shows three different strategies to handle CNTs. The first one is the dispersion-based processing[20,21], where CNT bundles are disassembled into individual tubes with the aid of surfactant covering, acid anion covering, or polymer wrapping. The main concern of this strategy is to overcome the intertube van der Waals (vdW) adhesion in CNT bundles, namely the bundling energy (E_{bundle}). The second strategy is the direct operation on CNT networks, where the problem locates on the rich CNT contacts, as reflected by the entanglement energy as the sum of the vdW interactions at CNT contacts, $E_{entangle} = \Sigma E_{contact}$. Three typical treatments to directly operate CNT networks are shown here, such as the direct stretching[22], contact lubricating with removable solvents[23], and contact welding with amorphous carbon[24,25]. These treatments show different results by modulating $E_{contact}$. The unmodulated yet high $E_{contact}$ causes straightening just for a partial fraction of CNTs upon stretching, which is insufficient to optimize the overall performance of the whole CNT assembly. The lubricating decreases $E_{contact}$ and thus allows a thorough aligning upon stretching. On the contrary, $E_{contact}$ can be strongly increased by covering amorphous carbon around CNT contacts, inducing a high elasticity for the CNT network.

Here, we report the third strategy to handle CNTs networks with an additional interaction via the introduction of branched polyethylenimine (PEI). This polymer has excellent affinity to CNTs[26] and multi-functionalities that can be applied in nanocomposites[27,28], bio-applications[29,30], neurotransmitters[31], electrochemical

sensing platform[32], n-type thermoelectric films[33], and so forth. Different from the linear PEI, which contains all secondary amines and is solid at room temperature, the branched PEI contains primary, secondary, and tertiary amino groups, and is liquid at all molecular weights[34]. By vacuum infiltrating branched PEI into CNT films, a CNT/polymer double network can be formed, and the CNT–polymer interaction ($E_{CNT-polymer}$) makes the CNTs much movable under the viscous dragging of liquid PEI. Therefore, the CNT movability can be strongly improved, leading to many novel and interesting features, especially remarkably enhanced viscoelasticity and ductility. It provides a facile method to align CNTs either by "passive" stretching or by "autonomous" creeping, offers an effective method to manipulate the mechanical properties of CNT films, and makes the CNT network repairable by reconstructing new networks with the aid of PEI.

Materials and methods

Synthesis of CNT film

The raw CNT films were synthesized by using FCCVD or iCVD[15–17,23,35,36]. A mixture solution containing acetone, ferrocene (0.5 wt%), and thiophene (1.0 wt%) was injected into a vertical ceramic tube furnace (diameter 100 mm) at a rate of 30 mL h^{-1} at 1300 °C. Consequently, entangled CNTs were grown and carried out by an Ar/H_2 gas flow with a volume ratio of 1:1 and flow rate of 5 L min^{-1}. The raw CNT films were formed by the layer-by-layer stacking of CNT aerogels, and the film thickness (10–12 μm) was controlled by the number of stacking layers.

Infiltration and removing of PEI and other polymers

Branched PEI with an average molecular weight of 10 kDa (Sigma-Aldrich Shanghai Trading Co. Ltd., Shanghai, China) was dissolved in ethanol at a concentration of 0.1 wt % for vacuum infiltration. A circular raw CNT film with a diameter of 8 cm was placed on a polycarbonate membrane, and then the PEI/ethanol solution was filtered through the raw CNT film. The obtained CNT/PEI composite film was washed with ethanol to remove the residual PEI on the film surface. The amount of infiltrated PEI was controlled by the volume of the PEI solution. For example, to realize the 25–50 wt% PEI mass fraction, the solution volume was about 300–500 mL.

Epoxy E51 and curing agent W93 (Xingchen Synthetic Material Co., Ltd., Nantong, China) were also used to impregnate CNT films. They were dissolved in acetone at a mass ratio of 10:3 and a total concentration of 50% (w/v). Long-chain alkyl silicone oil (SO, Iota Silicone Oil Co., Ltd., Bengbu, China) and PVA with a polymerization degree of 1750 (Sigma-Aldrich Shanghai Trading Co. Ltd., Shanghai, China) were dissolved in heptane and dimethyl sulfoxide (2 wt%), respectively, for the fabrication of CNT/SO and CNT/PVA composite films.

An electric current was conducted to pass through the CNT/PEI strip. Owing to the Joule-heating effect, the strip can be heated up to about 300 °C under a current density of 5–5.5 mA tex^{-1}[37]. The current was maintained for 10 min to remove PEI molecules as fully as possible.

Ductile stretching and tensile test

The PEI-infiltrated CNT film was cut into 0.5^{-1} cm × 5 cm strips for the stretching characterization performed with a ShengTe Tensile Tester (Intell-Rising Technology Co., Ltd., Suzhou, China) equipped with a 200-N load cell (precision 0.1 mN). A multi-step stretching[8] was applied; in every stretching step, the strip length was extended by 3–5% of the original length within 5 min, followed by a 10-min relaxation. The total stretching ratio was set to be 10–50%. The films were cut into 2 cm × 1 mm narrow strips for the tensile tests performed with an Instron 3365 UTM (Instron Corp, Norwood, USA) with a gauge length of 1 cm and tensile rate of 0.5 mm min^{-1}. The specific stress was evaluated to avoid the measurement error on the film thickness. A DMA 242 E Artemis (NETZSCH-Gerätebau GmbH, Selb, Germany) was used to characterize the dynamic properties. The vibration amplitude was controlled as load force variation and displacement variation in the two machines, respectively. The conversion between the different vibration amplitudes has been described elsewhere[38].

Characterizations

The sample morphology and microstructure were investigated by a field emission SEM (Quanta 400 FEG, FEI, Hillsboro, USA) and high-resolution TEM (Tecnai G2 F20 S-Twin, FEI, Hillsboro, USA). An FEI Scios Dual-Beam FIB was used to form the cross-sections and to take the cross-sectional images in SEM. The TGA test was conducted with a TGA-209 thermogravimetric analyzer (NETZSCH-Gerätebau GmbH, Selb, Germany) at a heating rate of 10 °C min^{-1} in nitrogen. The FTIR spectra were obtained with a Nicolet 6700 FTIR spectrometer (Thermo Scientific, Waltham, USA). The sheet resistance was measured with an ST2258C four-probe electro resistance analyzer (Jingge Electronics Co., Ltd., Suzhou, China). A Fotric 326Q-L25 Thermal Imager (Fotric Inc., Shanghai, China) was used to record the film temperature during the electric heating treatment, and the obtained sample was called as *I*-treated CNT/PEI film for short. The final PEI mass fraction was determined by the mass increase of the film and confirmed by TGA.

Results

Construction of CNT/PEI double network

CNT/PEI composite films were prepared by vacuum infiltrating PEI into CNT networks as schematically depicted in Fig. 2a and Supplementary Fig. S1, in which

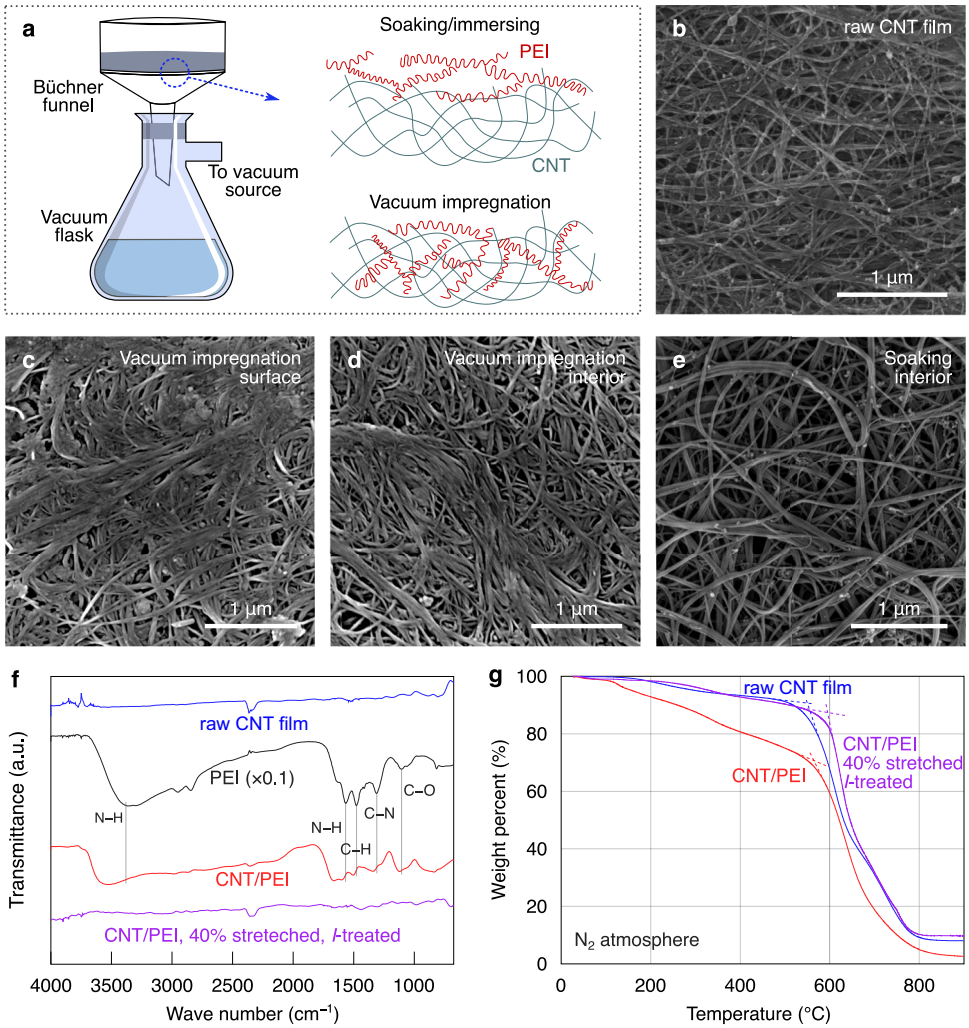

Fig. 2 Construction of CNT/PEI double network. a Schematic of the vacuum impregnation strategy which can promote the in-depth infiltration of PEI. **b** The raw CNT film with rich sub-μm pores. **c**, **d** Surface and interior morphologies of a PEI-infiltrated CNT film. **e** The interior morphology of a PEI solution-soaked CNT film. **f** TGA curves of the raw CNT film, CNT/PEI film, and the 40% stretched *I*-treated CNT/PEI film collected under nitrogen atmosphere. **g** FTIR curves of the raw CNT film, CNT/PEI film, and the 40% stretched *I*-treated CNT/PEI film, in which the characteristic peaks of different bond were marked.

CNT/PEI double network was formed. The vacuum infiltration is adopted because it can provide a driving force to penetrate PEI into raw CNT films. On the contrary, if raw CNT films are just soaked or immersed in the PEI solution, the big PEI molecules (average molecular weight of 10 kDa) will jam the sub-μm surface pores and interior spaces between CNT bundles, and thus cause to a very thin impregnation depth. The raw CNT films used here were synthesized through floating catalyst CVD (FCCVD, or called injection CVD, iCVD)[15–17,23,35,36]. The CNTs were mainly double- and triple-walled with diameters of 5–10 nm and aggregated to form bundles with diameters of 80–90 nm as shown by the scanning and transmission electron microscopies (SEM and TEM) images in Fig. 2b and Supplementary Fig. S2). Such long CNTs and bundles all entangled with each other to build up a strong and tough network Such high entanglement can avoid CNT aggregation during the liquid densification and polymer impregnation process[8].

To achieve an efficient infiltration, the branched PEI was dissolved in ethanol at a low concentration. When the concentration exceeded 0.5 wt%, PEI molecules would jam the surface pores and thus suppress the inside impregnation. Dilute PEI solutions with concentrations from 0.1 to 0.2 wt% were able to induce a high level of in-depth infiltration, whereas the infiltrated PEI was too low if the solution concentration was further decreased. However, PEI was overloaded in the CNT film when the concentration was 0.2 wt%, as reflected by the thick covering on film surfaces (Supplementary Fig. S3). So, the

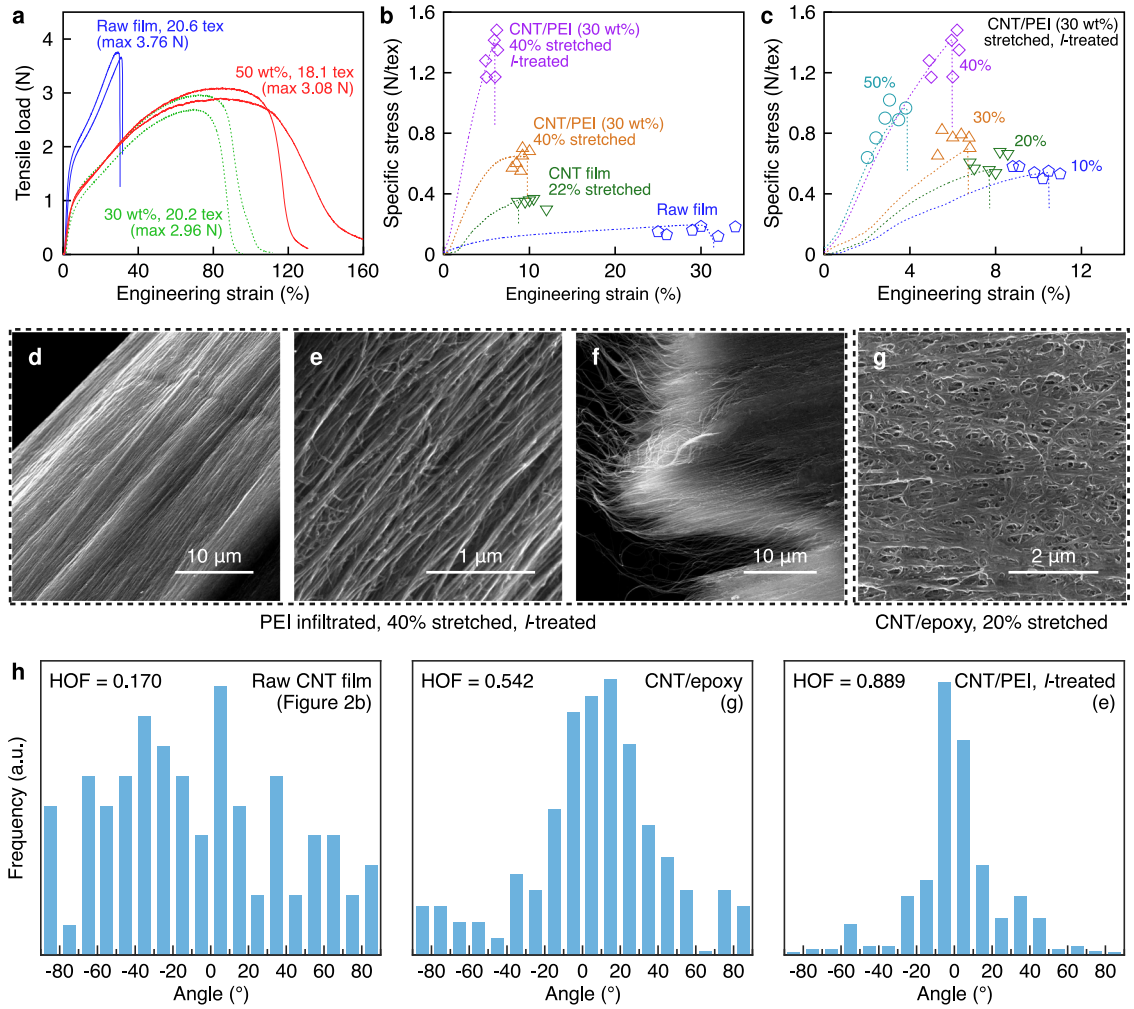

Fig. 3 Ductility-induced stretching and strengthening. a Tensile load–stress curve showing the significantly enhanced of ductility of CNT/PEI double network. **b** Effect of stretching, PEI infiltration (30 wt%), and electric heating treatment on the tensile behaviors. **c** Effect of stretching ratio on the tensile properties of CNT/PEI composite. **d**–**f** Morphologies of the 40% stretched and *I*-treated CNT/PEI composite. The high alignment degree and the short sliding distance (10–20 μm) at the fracture region reflected a strong intertube adhesion. **g** The morphology of the 20% stretched CNT/epoxy film, in which the weak viscous drag remained the entangled network structure. **h** The Herman's orientation factors of the raw CNT film in Fig. 2b, the stretched CNT/epoxy film (**g**), and the *I*-treated and stretched CNT/PEI film (**e**), respectively.

optimal concentration was 0.1 wt% and the mass content of PEI was controlled by the solution volume. For example, the final PEI fraction was about 25 and 50 wt% when 300- and 500-ml solutions were used, respectively. To show the efficient inside infiltration, the CNT/PEI film was peeled with adhesive tape for several times, until the half film thickness, to show the interior morphology. As shown in Fig. 2c, d, the same mushy morphology clearly shows that PEI was efficiently infiltrated into the interior of the film, leading to the adhesion between neighboring CNT bundles. On the contrary, soaking the raw CNT film in PEI solutions did not show an evident inside infiltration as reflected by the neat and sharp morphology (Fig. 2e). Fourier transform infrared spectroscopy (FTIR) was used to further confirm the existence of PEI. Note that the organic by-product of the iCVD fiber – dioctyl phthalate (DOP, $C_{24}H_{38}O_4$, 7–9 wt%[35]) can be removed during the vacuum infiltration process and the iron catalyst (3–7 wt%) has very limited influence on the spectrum. The characteristic peaks observed in Fig. 2g) are all ascribed to the PEI molecule, including C-O stretching, C-N stretching, C-H bending, and N-H bending between 1000 and 1600 cm^{-1} and amine N-H stretching mode around 3530 cm^{-1}. Moreover, these peaks all blueshifted to higher wavenumbers when compared to the pure PEI, especially for the N-H stretching mode (originally around 3360 cm^{-1}). This observation reflects the effective interaction between CNTs and PEI molecules, which increases the energy cost for N-H stretching due to the intimate adhesion between amine groups and CNT sp^2 surfaces[39].

Then, the mass content of infiltrated PEI was confirmed by thermogravimetric analysis (TGA), see Figs. 2f and Supplementary Fig. S4. PEI evaporated or decomposed at the maximum speed at about 420 °C and were fully removed when the temperature reached 550 °C. The content of PEI calculated from the weight loss is 30 wt% in the composite film obtained with an optimal impregnation. Also, the FTIR, TGA, and DTG results all confirm that the infiltrated PEI can be fully removed by an electric heating treatment, consistent with the work of Qiu et al[37]. At a current of 5.5 mA tex^{-1} (110 mA current through a 20 tex CNT/PEI strip), the film temperature could reach 300 °C (Supplementary Fig. S5), higher than the boiling point of PEI (≈250 °C) and in the range of decomposition temperature (T_{decomp} ≈ 270–320 °C) of PEI[40]. Hence, after a 10 min electric heating treatment, PEI molecules were fully evaporated or decomposed as reflected by the recovered TG curve with no characteristic peaks of PEI (Fig. 2f, g).

Enhanced ductility and stretching-based strengthening

High ductility is achieved in the formed CNT/PEI with uniform PEI impregnation. To show this, Fig. 3a compares the tensile load–strain curves of the raw CNT films and the CNT/PEI composite films with a similar linear mass density of 18–21 tex (g km^{-1}) by cutting the films into long and narrow strips (see Methods). Although all these films all exhibited an elastic deformation in the initial stretching stage and then a plastic region, the CNT/PEI composite film exhibited superior stretchability as reflected by the high strain at break, which is the intuitive representation of high ductility. For example, the 30 wt% PEI infiltration increased the breaking strain up to 80–86% while the maximum tensile load appeared at a strain of around 65%. The CNT alignment was remarkably improved by such ductile stretching as mentioned below. However, the contacts between CNTs were softened by the PEI molecules, making the stress (0.15 N tex^{-1}) slightly smaller than the raw film (0.18 N tex^{-1}). This issue can be resolved by the electric heating treatment to remove PEI molecules and thus recover the strong CNT–CNT adhesion. So, the introduction of PEI provides a feasible method to modulate the static mechanical properties of CNT assemblies. When 30 wt% PEI was infiltrated, the raw CNT film first became "wetted" by PEI and had a reduced strength (Fig. 3a). Then the CNT/PEI film was strengthened to 0.55–0.70 N tex^{-1} by the 40% stretching owing to the greatly improved alignment of CNTs. After a further electric heating treatment to remove PEI, the stretched film got "dried" and further strengthened. At a current density of 5.5 mA tex^{-1}, the *I*-treated film reached the highest strength of 1.18–1.49 N tex^{-1} (Fig. 3b). In comparison, the 22% stretched raw CNT film could just increase its strength from 0.19 to 0.37 N tex^{-1}, and there is no more room to further increase the stretching ratio and thus the strength of the raw CNT film. Besides, the optimal PEI mass fraction was about 30 wt% by the overall consideration of the mass density and the tensile properties of stretched CNT films (see the comparison of the stress–strain curves between different samples shown in Supplementary Fig. S6).

The stretching level is critical in determining the final mechanical performance of the *I*-treated CNT/PEI film. As shown in Fig. 3c, when the stretching ratio increased from 10 to 40% with a step of 10%, the tensile strength was elevated to 0.50–0.58, 0.54–0.68, 0.65–0.82, and 1.18–1.49 N tex^{-1}, respectively. Meanwhile, the strain at break gradually decreased from 9.6% to 5.7%. The over stretching of 50% could further increase the modulus but made the final stretched and *I*-treated film brittle (strain at break ≈2.9%), leading to the decrease in strength (down to 0.64–1.02 N tex^{-1}). Hence, 40% is the optimal stretching ratio and chosen to get the best static mechanical performance. This increased tensile strength originated from the highly improved alignment of CNTs. Figure 3d, e clearly show that the CNT bundles were well oriented along one direction. In order to provide a quantitative description of the alignment, Herman's orientation factor (HOF)[8,41] was calculated for the raw (Fig. 2b) and the highly stretched films (Fig. 3e), as shown in Fig. 3h. Details of the HOF calculation are provided in Supplementary Fig. S7. The HOF takes the value 1 for a system with a perfect orientation parallel to the reference direction, and zero for a completely non-oriented system. For the raw CNT film, the HOF was as small as 0.170, and it rose to 0.889 after the PEI-assisted stretching. These values well reflect that the alignment was greatly improved in the stretched CNT film with the help of PEI. Hence, the CNT/PEI double network offers an effective method to improve the mechanical performance of CNT films by the highly manipulable microstructure.

The variation in film resistance offers a side-view of the nano-structural change during the sequential operations, i.e., PEI infiltration – stretching – electric heating treatment. The raw CNT film exhibited a sheet resistance of 2.54–2.86 Ω □$^{-1}$ (Supplementary Fig. S8). The direct stretching improved the CNT alignment, but the CNTs might separate from each other at connection nodes during the stretching, resulting in a slight increase in resistance (2.64–2.89 Ω □$^{-1}$). With the infiltrated PEI, the resistance increased to 3.12–3.54 Ω □$^{-1}$ because that a certain number of electron transport pathways between CNTs were blocked by this nonconductive polymer. However, after the 40%-stretching, the film resistance maintained nearly the same (3.15–3.59 Ω □$^{-1}$), showing that the connection nodes between CNTs were not destroyed during the PEI-assisted stretching treatment. Then, after the electric heating treatment, the conductivity

recovered to its original level (2.47–2.80 Ω $\square^{-1}$) owing to the drawing-together of CNTs by the leaving PEI and the attractive force between two parallel currents passing through the CNTs. So, the recovered conductivity reveals the reconstructed contacts between CNTs, consistent with the improved mechanical performance of the stretched and *I*-treated CNT/PEI films.

Figure 3f shows the fracture morphology of a stretched and *I*-treated CNT/PEI film. CNTs slid against each other by a certain sliding distance, $l \approx 20\,\mu m$. This value was used to estimate the interfacial shear strength σ_i between CNTs. By assuming that the CNT bundles with a diameter of $D_{bundle} = 80\,nm$ are hexagonally packed, the bundle strength σ should satisfy $\sigma_i \pi D_{bundle} l = \sigma\pi(D_{bundle}/2)^2$. Therefore, σ_i is estimated to be about 20–40 MPa by using $\sigma = 10–20\,GPa$ according to experimental measurements[42,43]. Such an exciting value is a rational result of the high CNT alignment, and it is close to theoretical estimations[44], consistent with the high tensile strength.

To show the superiority of our CNT/PEI double network, the infiltration agent was also replaced by epoxy resins (E51) with a mass fraction of 40 wt%. Unfortunately, the breaking strain of the obtained CNT/epoxy was only 15–20%, during which the CNTs could not be effectively stretched and aligned as shown in Fig. 3g. The corresponding HOF was just 0.542 (Fig. 3h), much lower than the value achieved in CNT/PEI film (0.889). This comparison inversely reflected that the CNT/PEI double network is critical in realizing the high ductility and thus improving of the static mechanical property of CNT films.

Viscoelasticity and creeping-based strengthening

As PEI is a viscous material and can soften the connection between CNTs, it can also endow the CNT/PEI composite film with greatly improved viscoelasticity. To be specific, after the PEI infiltration, new connection nodes between CNTs and PEI molecules were formed, which is much more viscous than the CNT–CNT

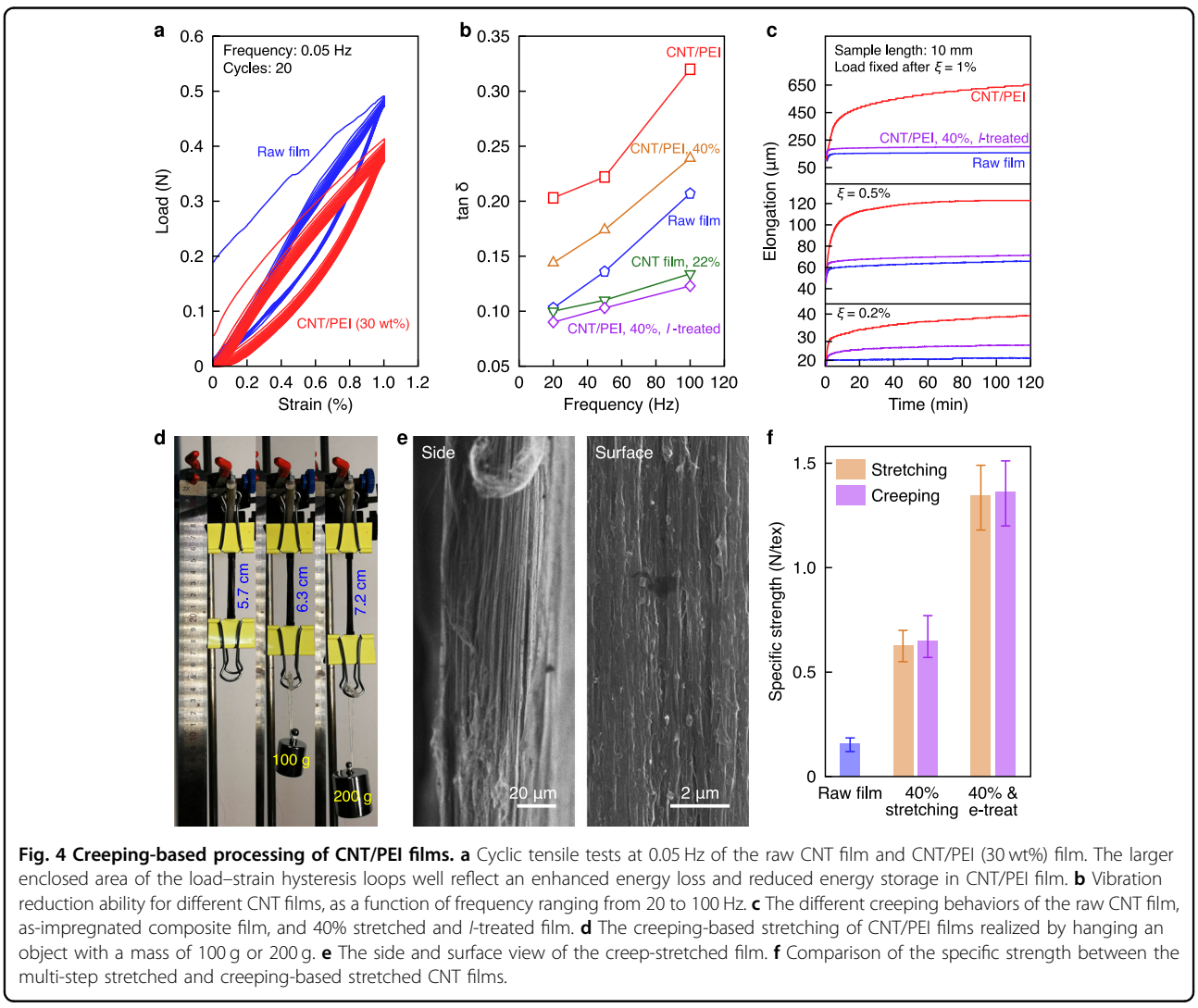

Fig. 4 Creeping-based processing of CNT/PEI films. a Cyclic tensile tests at 0.05 Hz of the raw CNT film and CNT/PEI (30 wt%) film. The larger enclosed area of the load–strain hysteresis loops well reflect an enhanced energy loss and reduced energy storage in CNT/PEI film. **b** Vibration reduction ability for different CNT films, as a function of frequency ranging from 20 to 100 Hz. **c** The different creeping behaviors of the raw CNT film, as-impregnated composite film, and 40% stretched and *I*-treated film. **d** The creeping-based stretching of CNT/PEI films realized by hanging an object with a mass of 100 g or 200 g. **e** The side and surface view of the creep-stretched film. **f** Comparison of the specific strength between the multi-step stretched and creeping-based stretched CNT films.

connection. The contact between CNTs is simply a point-to-point or coarse grain-to-grain vdW interaction. It is pretty strong due to $\pi-\pi$ stacking between the sp^2 lattices but too brittle to sustain large deformations[5]. On the contrary, the CNT–PEI connections are much softer owing to the following reasons: First, the branched long chains can wrap around CNTs and allows a larger sliding distance between CNTs or bundles before their separation[5,35,45], corresponding to an increased sliding energy dissipation. Second, the PEI molecules are inherently much more viscous as compared to the rigid CNT structure, contributing to the high internal viscosity of the CNT/PEI double network. Third, the long-chain and branched structure of PEI can induce coherent vibrational coupling for non-adjacent CNTs.

Therefore, the CNT/PEI composite film became quite viscoelastic with high vibration reduction ability, as reflected by the cyclic tensile tests with a small strain of 1% (Fig. 4a). Compared to the raw CNT film, the enclosed area of the stress–strain cycles became much larger, corresponding to the enhanced damp vibration ability of the CNT/PEI film. The loss tangent (tan δ), i.e., the ratio of loss modulus to storage modulus, was calculated to quantitatively describe the viscoelasticity. The raw CNT film had a loss tangent of 0.103, 0.136, and 0.207 at 20, 50, and 100 Hz, respectively (Fig. 4b). With the infiltrated PEI, the damping ability increased remarkably, up to tan $\delta = 0.203$, 0.222, and 0.320 at the same frequencies. Such damping property is comparable to silicone rubber (one of the most commonly used damping materials with tan $\delta \approx 0.3$). Besides, the as-produced CNT/PEI composite film had a high modulus of 200 MPa (Fig. 3a), two orders of magnitude higher than that of silicone rubber (≈1 MPa). So, the CNT/PEI composite film become a promising high-performance cushioning material.

The high viscoelasticity also facilitated the stretching of the CNT/PEI film by a creep deformation. To show the availability, Fig. 4c compares the different creep behaviors of the raw CNT and CNT/PEI films. The samples were first stretched to a given strain of 0.2%, 0.5%, or 1%, and then the tensile load was kept as constant. For example, when fixing the load after the 0.5% pre-stretching, the fiber elongated, and the elongation increased from 50 μm to 118 μm in 40 min for a 10 mm long CNT/PEI film. As a contrast, the final increase was just 63 μm and 69 μm for the raw and *I*-treated samples, respectively. The elongation became much higher when the first stretching increased to 1%; the CNT/PEI film could get elongated by more than 550 μm (>5.5%) in 1 h. This creeping deformation was directly shown in Fig. 4d. The CNT/PEI strip extended its length by about 10.5% and 26.3% with an object hung on the tail end. From the side and surface views of the creep-stretched CNT/PEI film (Fig. 4e), it was confirmed that the CNTs here were highly aligned by the creep-stretching. The calculated HOF factor was 0.891, as the same as the stretched sample. With the improved alignment, this creeping treatment showed a similar strengthening effect as the aforementioned stretching. Figure 4f shows that with the same elongation ratio of 40%, the two treatments yielded nearly the same strength either with PEI (0.63–0.65 N tex^{-1}) or after the electric heating treatment (1.20–1.51 N tex^{-1}). The creeping was even slightly better because full structural relaxation was realized during the creeping elongation process.

However, the stretching treatment degrades the damping performance of CNT films because of the improved alignment (Fig. 4b). The weakest damping ability, with a loss tangent of 0.123–0.134 at 100 Hz, was observed in the stretched raw CNT films and the stretched and *I*-treated CNT/PEI films. The frequency dependence was also different for the unstretched and stretched films with different microstructures (entangled and aligned, respectively). The loss tangent increased very rapidly with frequency for the entangled CNT and CNT/PEI films, whereas it increased slowly for the aligned films, in agreement with the phenomenon observed in CNT fibers[38,45]. Hence, this PEI-based engineering mentioned in this work can significantly modulate both the quasi-static and dynamic mechanical properties of CNT assemblies.

Repairability

The superb ductility and viscoelasticity lead to another important processing ability –repairability in the CNT/PEI double networks. It is reminiscent of a Chinese conventional handicraft, pot mending, to repair a broken pot, kettle, or basin by hammering the juncture to reconstruct the two pieces of the pot as shown in Fig. 5a. Inspired by this, the repair/healing of CNT films was performed to sew two separate CNT networks together via the molecular motion of PEI chains, see Fig. 5b. First, PEI/ethanol solution (w/v 1%) was dipped onto the broken parts to wet and soften the CNT films. Then a similar "hammering" treatment was used, i.e., rubbing the films with a finger just like massaging human skins. Owing to the high viscoelasticity, PEI chains would move under the external shear stress and thus drag the neighboring CNTs to follow the motion, leading to the reconstruction of CNT networks. In our previous study, PEI has been successfully applied to unite multiple CNT fibers into an individual yarn with eliminated inter-fiber contacts, showing such reconstruction ability[46]. The CNT/PEI film also exhibited similar superior ductility under hammering to ensure the structural reconstruction as reflected in Fig. 5c and Supplementary Fig. S9. Both the length and width dimensions extended by more than 30% under hammering. On the contrary, the film broke without PEI, forming many broken holes. On the microscale, CNTs were still connected

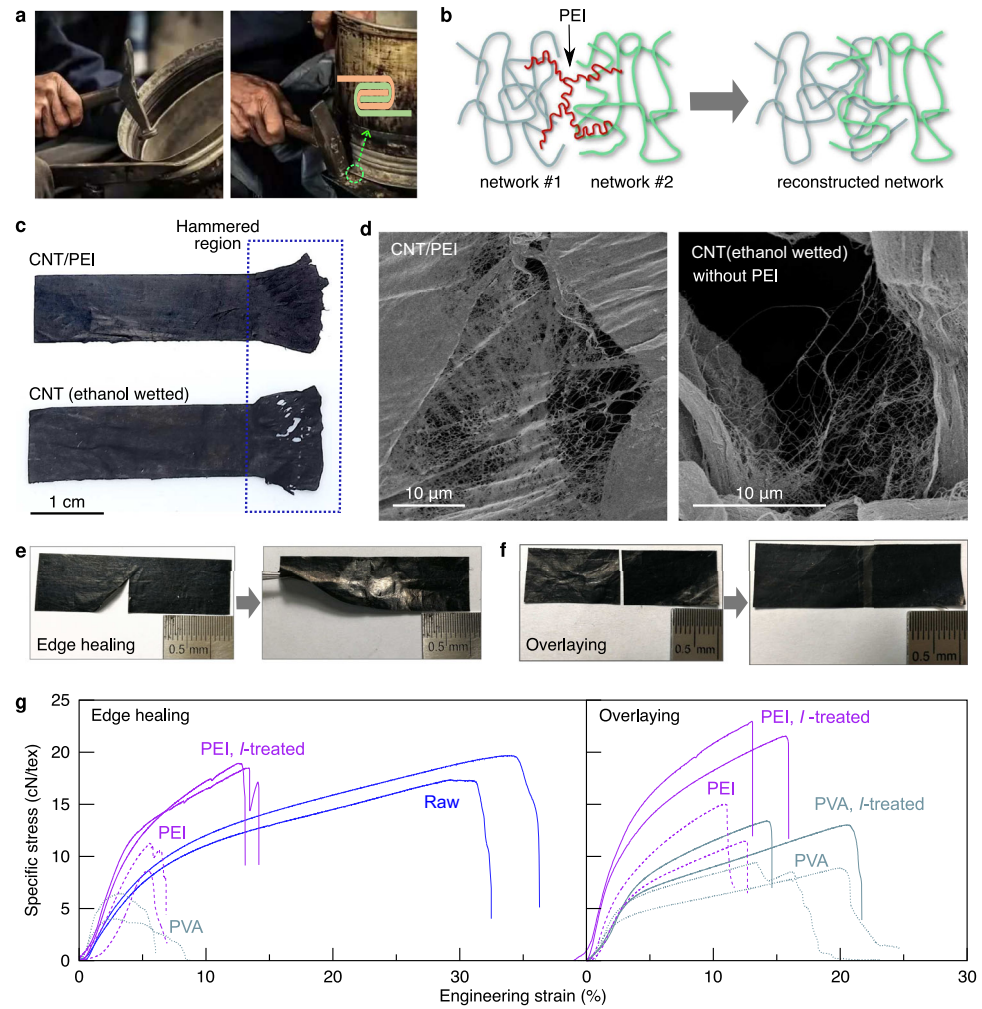

Fig. 5 Repair of fractured CNT films. a The traditional Chinese handicraft – Hammering irons to repair/mend the broken pots[50]. And the inset shows (**b**) Schematic of the CNT network reconstruction driven by the motion of PEI molecules. **c** Comparison between the CNT/PEI and ethanol wetted CNT films after being "hammered". The different morphologies clearly show the high ductility of CNT/PEI film under hammering. **d** SEM images showing the ductile deformation and torn-apart morphology of the hammered CNT films with and without PEI. CNT films before and after the edge healing (**e**) and overlaying healing (**f**). **g** Comparison of the tensile strain behavior of the raw CNT film, the edge- and overlaying-healed CNT films with the infiltrated PEI or PVA before and after the electric heating treatment.

with each other with a large deformation in the CNT/PEI film, whereas CNTs detached from each other after rubbing in the raw CNT film (Fig. 5d). More examples are provided in Supplementary Fig. S10 to show the ubiquity. So, the CNT/PEI double network could undergo larger strains without being broken, which endows it with high repairability than the fragile raw CNT film.

Two different ways of film repair/healing, i.e., edge healing and overlaying healing, were successfully realized, see Fig. 5e, f. Generally speaking, the edge healing is more suitable for a thick film while the overlaying is better for a thin film. However, the as-repaired films were weak due to the presence of PEI. As shown in Fig. 5f, the as-repaired films fractured at a small stress of 8.7–11.3 cN tex^{-1}, smaller than the fracture strength of the raw film 17.3–19.6 cN tex^{-1}. By applying a current of 5–5.5 mA tex^{-1} to remove PEI, the contact between the joint films became strengthened to solidify the reconstructed CNT network. Thus, the healed film showed a full recovery of strength of 18.5–19.1 cN tex^{-1} (Fig. 5f). The overlaying treatment showed a similar healing effect. Before and after the current treatment, the repaired films exhibited fracture stresses of 11.5–15.0 and 21.6–23.1 cN tex^{-1}, respectively (Fig. 5f), stronger than the side edge healing films.

The long-chain, viscous, and branched PEI play a critical role in the healing process. This long-chain polymer can interact with CNTs and cause a drag force to activate

the motion of CNTs, and its high viscosity ensures the continuous motion. More importantly, the branched structure of PEI can effectively hinder the sliding between CNT and polymer due to the enriched crossed junctions. As a comparison, poly(vinyl alcohol) (PVA, polymerization degree 1750), dissolved in water at a concentration of 1% (w/v), was used to repair fractured CNT films. Unfortunately, the side-edge adhesion easily fractured at a stress of 4.0–6.4 cN tex^{-1}, and the overlaying one also exhibited a limited strength of 8.9–9.4 cN tex^{-1}. The current treatment to remove PVA did not work for these samples, it just increased the fracture stress to only 13.0–13.5 cN tex^{-1}. Such comparison clearly revealed that CNT networks could be just efficiently reconstructed by PEI.

To show the healing effect, focused ion beam (FIB) was used to characterize the microstructure of the cross-section of the repaired segment, see Fig. 6. The seam between the jointed two films was eliminated in the edge healing sample (Fig. 6a). For the overlayed healing, the samples healed with PEI and PVA were shown in Fig. 6b, c. Obviously, the PEI-based healing well eliminated the seam between the up and down films, whereas a conspicuous seam was still observed in the healed CNT/PVA sample. Such a difference well explained the different mechanical stresses of the healed CNT/PEI and CNT/PVA films, and thus confirms the effectiveness of PEI infiltration in the healing/repair of CNT assemblies.

Discussion

High ductility is the key to achieve the stretching-induced strengthening and healing of CNT films. Three elements, i.e., the long chains, high viscosity, and branched structure of infiltrated PEI molecules, are essential to realize such high ductility. Specially, the branched structure facilitates the formation of a CNT/PEI double network and thus exerts the full potential of the high viscosity of this composite.

As the linear PEI is solid at room temperature (melting point higher than 67 °C for the linear PEI with the similar molecular weight), so to show the advantage of branched polymers, a viscous yet non-branched polymer – long-chain linear polysiloxanes or commonly known as silicone oil (SO) was used to infiltrate raw CNT films. The CNT/SO composite film did not show viscoelasticity but a slippery behavior as its length continuously increased even under a small external load until it fractured (Fig. 7). This is obviously different from the creeping behavior of the viscoelastic CNT/PEI film. More importantly, after being stretched, the CNTs in the CNT/SO film were still not aligned (7c), totally different from the situation in CNT/PEI film (Figs. 3d–f and 4e). This contrast clearly reveals the great effect of the branched structure on the rearrangement of CNTs and thus the strengthening of CNT films as well as the repairing of broken CNT assemblies.

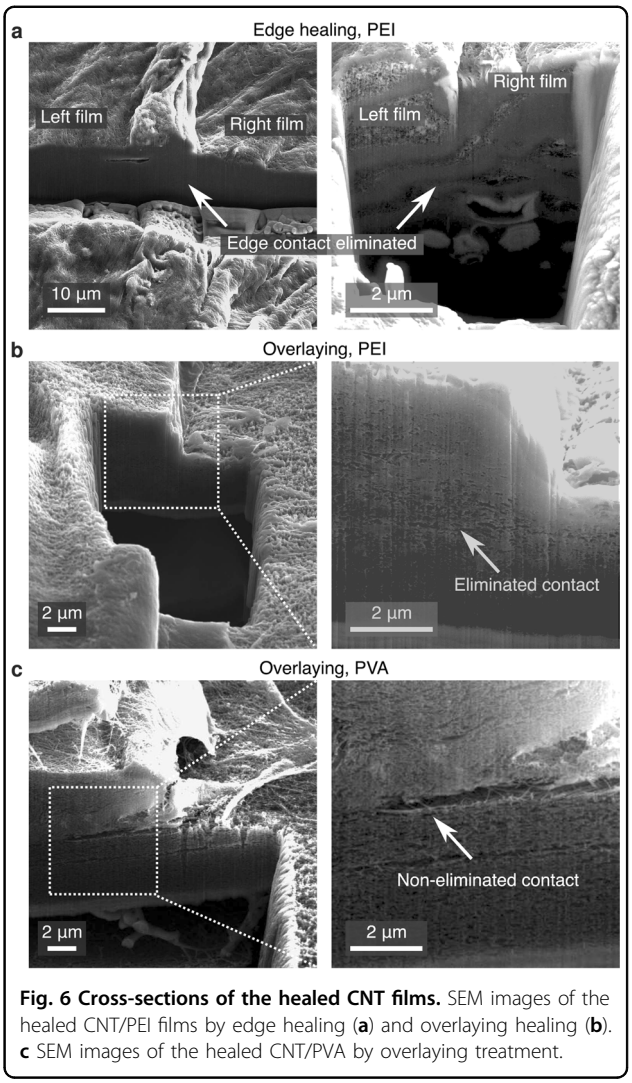

Fig. 6 Cross-sections of the healed CNT films. SEM images of the healed CNT/PEI films by edge healing (**a**) and overlaying healing (**b**). **c** SEM images of the healed CNT/PVA by overlaying treatment.

Other polymers, e.g., ultrahigh molecular weight polyethylene, was introduced into CNT fibers to realize a similar polymer-assisted stretching[47]. However, due to the lack of the branched polymeric structure, it requires not only a high amount of polymer (more than 70 wt%) but also an extremely high stretching of 600–1000% to achieve the similarly improved alignment of CNTs. In another work, click reaction was implemented to graft thiol-ended hyperbranched polymers on CNTs[48]. Such grafting generated a composite structure close to the CNT/PEI double network and allowed for the deformation and slip between CNTs toward a remarkably improved CNT alignment. A different double network was also realized between long-chain polymer PVA (1D) and sulfonated graphenal polymer (2D)[49]. This double network is highly hydrophilic and thus shows superior repairability with the aid of water wetting.

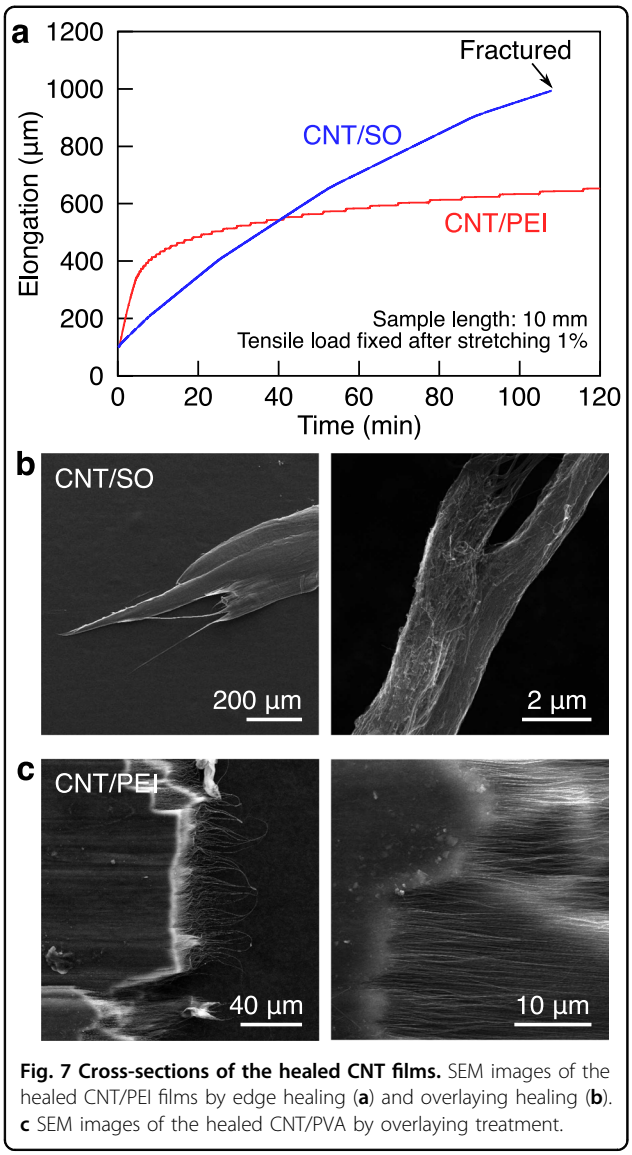

Fig. 7 Cross-sections of the healed CNT films. SEM images of the healed CNT/PEI films by edge healing (**a**) and overlaying healing (**b**). **c** SEM images of the healed CNT/PVA by overlaying treatment.

In conclusion, branched PEI was vacuum infiltrated into raw CNT films, making them highly viscoelastic, ductile, and thus repairable with the formation of CNT/PEI double network. It offers a new method to modulate the microstructure of CNT assemblies. High alignment of CNTs was realized through the PEI-assisted stretching or creeping deformation, and structural reconstruction of different CNT/PEI double networks were also accomplished via a hammering treatment. Hence, strengthening or repairing of CNT films were fulfiled through the sequence of operations, i.e., PEI infiltration – stretching/creeping or hammering treatment – electric heating treatment. This strategy exhibits a strengthening ability even better than the commonly used stretching method and will become an effective means to manipulate carbonene material in the future.

Acknowledgements
The authors gratefully acknowledge financial supports from the Fundamental Research Funds for the Central Universities (2232021G-01), National Natural Science Foundation of China (51561145008, 51862036, 62176158, 52202044), and Suzhou Science and Technology Program for Industrial Prospect and Key technology grant SYC2022018. X.H.Z. thanks Chunyang Jiang for her suggestion to consider polyethylenimine for impregnation, and acknowledges discussions with Professor Xuetong Zhang

Author details
[1]Innovation Center for Textile Science and Technology, College of Textiles, and MOE Key Laboratory of Textile Science & Technology, Donghua University, Shanghai 201620, China. [2]Advanced Materials Division, and Key Laboratory of Multifunctional Nanomaterials and Smart Systems, Suzhou Institute of Nano-Tech and Nano-Bionics, Chinese Academy of Sciences, Suzhou 215123, China. [3]School of Physical Science and Technology, Suzhou University of Science and Technology, Suzhou 215009, China. [4]Division of Nanomaterials, and Jiangxi Key Lab of Carbonene Materials, Jiangxi Institute of Nanotechnology, Nanchang 330200, China

Author contributions
X.H.Z., J.Y.Z. and J.N.Z. conceived the idea and designed the research. X.H.Z., X.W., X.Z., J.Y.Z., and J.N.Z. conducted the experiments and performed data analyses. Y.Y.Z. assisted the sample preparation and characterization. X.H.Z. and Q.W.L. supervised the study. X.H.Z. wrote the manuscript. And all the authors discussed the results and commented on the manuscript.

Conflict of interest
The authors declare no competing interests.

Supplementary information The online version contains supplementary material available at https://doi.org/10.1038/s41427-023-00490-z.

Received: 6 February 2023 Revised: 30 May 2023 Accepted: 20 June 2023.
Published online: 11 August 2023

References

1. Blaiszik, B. J. et al. Self-healing polymers and composites. *Annu. Rev. Mater. Res.* **40**, 179–211 (2010).
2. Ha, T. L. B., Quan, T. M., Vu, D. N., & Si, D. M. in *Regenerative Medicine and Tissue Engineering* (ed. Andrades, J. A.) Ch. 11 (IntechOpen, 2013).
3. Wegst, U. G. K., Bai, H., Saiz, E., Tomsia, A. P. & Ritchie, R. O. Bioinspired structural materials. *Nat. Mater.* **14**, 23–36 (2015).
4. Wang, Y., Pham, D. T. & Ji, C. Self-healing composites: a review. *Cogent Eng.* **2**, 1075686 (2015).
5. Naraghi, M. et al. A multiscale study of high performance double-walled nanotube–polymer fibers. *ACS Nano* **4**, 6463–6476 (2010).
6. Beese, A. M. et al. Bio-inspired carbon nanotube–polymer composite yarns with hydrogen bond-mediated lateral interactions. *ACS Nano* **7**, 3434–3446 (2013).
7. Cheng, Q., Jiang, L. & Tang, Z. Bioinspired layered materials with superior mechanical performance. *Acc. Chem. Res.* **47**, 1256–1266 (2014).
8. Han, Y. et al. Bio-inspired aggregation control of carbon nanotubes for ultra-strong composites. *Sci. Rep.* **5**, 11533 (2015).
9. Zhang, X., Yu, X., Zhao, J. & Li, Q. in *Carbon nanotubes – current progress of their polymer composites* (ed. Berber, M. R. & Hafez, I. H.), Ch. 3 (IntechOpen, 2016).
10. Luo, C., Li, F., Li, D., Fu, Q. & Pan, C. Bioinspired single-walled carbon nanotubes as a spider silk structure for ultrahigh mechanical property. *ACS Appl. Mater. Interfaces* **8**, 31256–31263 (2016).
11. Liu, L., Ma, W. & Zhang, Z. Macroscopic carbon nanotube assemblies: preparation, properties, and potential applications. *Small* **7**, 1504–1520 (2011).

12. Lin, Z. et al. Carbon nanotube sponges, aerogels, and hierarchical composites: Synthesis, properties, and energy applications. *Adv. Energy Mater.* **6**, 1600554 (2016).
13. Sui, X. et al. Multilevel composite using carbon nanotube fibers (CNTF). *Compos. Sci. Technol.* **137**, 35–43 (2016).
14. Kinloch, I. A., Suhr, J., Lou, J., Young, R. J. & Ajayan, P. M. Composites with carbon nanotubes and graphene: an outlook. *Science* **362**, 547–553 (2018).
15. Li, Y.-L., Kinloch, I. A. & Windle, A. H. Direct spinning of carbon nanotube fibers from chemical vapor deposition synthesis. *Science* **304**, 276–278 (2004).
16. Wang, J. N., Luo, X. G., Wu, T. & Chen, Y. High-strength carbon nanotube fibre-like ribbon with high ductility and high electrical conductivity. *Nat. Commun.* **5**, 3848 (2014).
17. Janas, D. & Koziol, K. K. Carbon nanotube fibers and films: synthesis, applications and perspectives of the direct-spinning method. *Nanoscale* **8**, 19475–19490 (2016).
18. Wagner, H. D. Paving the way to stronger materials. *Nat. Nanotechnol.* **2**, 742–744 (2007).
19. Zhang, X. in *Nanomechanics* (ed Vakhrushev, A.) Ch. 1 (IntechOpen, 2017).
20. Ma, P.-C., Siddiqui, N. A., Marom, G. & Kim, J.-K. Dispersion and functionalization of carbon nanotubes for polymer-based nanocomposites: a review. *Compos. Part A Appl. Sci. Manuf.* **41**, 1345–1367 (2010).
21. Jiang, Y., Song, H. & Xu, R. Research on the dispersion of carbon nanotubes by ultrasonic oscillation, surfactant and centrifugation respectively and fiscal policies for its industrial development. *Ultrason. Sonochem.* **48**, 30–38 (2018).
22. Cheng, Q. et al. High mechanical performance composite conductor: multi-walled carbon nanotube sheet/bismaleimide nanocomposites. *Adv. Funct. Mater.* **19**, 3219–3225 (2009).
23. Wang, J. et al. Shampoo assisted aligning of carbon nanotubes toward strong, stiff and conductive fibers. *RSC Adv.* **10**, 18715–18720 (2020).
24. Wang, H. et al. Ultra-lightweight and highly adaptive all-carbon elastic conductors with stable electrical resistance. *Adv. Funct. Mater.* **27**, 1606220 (2017).
25. Chen, Z. et al. Developing elastic, robust, and highly porous metal foams using carbon nanotube scaffolds. *ACS Appl. Electron Mater.* **2**, 2090–2097 (2020).
26. Friddle, R. W. et al. Single functional group interactions with individual carbon nanotubes. *Nat. Nanotechnol.* **2**, 692–697 (2007).
27. Muñoz, E. et al. Highly conducting carbon nanotube/polyethyleneimine composite fibers. *Adv. Mater.* **17**, 1064–1067 (2005).
28. Robert, C. et al. Improving through-thickness conductivity of carbon fiber reinforced polymer using carbon nanotube/polyethylenimine at the inter-laminar region. *J. Appl. Polym. Sci.* **138**, 49749 (2021).
29. Liu, Y. et al. Polyethylenimine-grafted multiwalled carbon nanotubes for secure noncovalent immobilization and efficient delivery of DNA. *Angew. Chem. Int. Ed.* **44**, 4782–4785 (2005).
30. Foillard, S., Zuber, G. & Doris, E. Polyethylenimine–carbon nanotube nanohybrids for siRNA-mediated gene silencing at cellular level. *Nanoscale* **3**, 1461–1464 (2011).
31. Zestos, A. G., Jacobs, C. B., Trikantzopoulos, E., Ross, A. E. & Venton, B. J. Polyethylenimine carbon nanotube fiber electrodes for enhanced detection of neurotransmitters. *Anal. Chem.* **86**, 8568–8575 (2014).
32. Duan, S., Yue, R. & Huang, Y. Polyethylenimine-carbon nanotubes composite as an electrochemical sensing platform for silver nanoparticles. *Talanta* **160**, 607–613 (2016).
33. Zhou, W. et al. High-performance and compact-designed flexible thermoelectric modules enabled by a reticulate carbon nanotube architecture. *Nat. Commun.* **8**, 14886 (2017).
34. Kobayashi, S., Shirasaka, H., Suh, K.-D. & Uyama, H. Viscosity behaviors and gel properties of linear and branched polyethylenimines: effects of microstructures. *Polym. J.* **22**, 442–446 (1990).
35. Zou, J. et al. Strengthening and toughening effects by strapping carbon nanotube cross-links with polymer molecules. Compos. *Sci. Technol.* **135**, 123–127 (2016).
36. Zhou, T. et al. The synergetic relationship between the length and orientation of carbon nanotubes in direct spinning of high-strength carbon nanotube fibers. *Mater. Des.* **203**, 109557 (2021).
37. Qiu, L. et al. Electro curing of oriented bismaleimide between aligned carbon nanotubes for high mechanical and thermal performances. *Carbon* **145**, 650–657 (2019).
38. Zhao, J., Zhang, X., Pan, Z. & Li, Q. Wide-range tunable dynamic property of carbon-nanotube-based fibers. *Adv. Mater. Interfaces* **2**, 1500093 (2015).
39. Díez-Pascual, A. M. & Díez-Vicente, A. L. Nano-TiO_2 reinforced PEEK/PEI blends as biomaterials for load-bearing implant applications. *ACS Appl. Mater. Interfaces* **7**, 5561–5573 (2015).
40. Nedel'ko, V. V., Korsunskii, B. L., Dubovitskii, F. I. & Gromova, G. L. The thermal degradation of branched polyethylenimine. *Polym. Sci. U.S.S.R.* **17**, 1697–1703 (1975).
41. Xu, M., Futaba, D. N., Yumura, M. & Hata, K. Alignment control of carbon nanotube forest from random to nearly perfectly aligned by utilizing the crowding effect. *ACS Nano* **6**, 5837–5844 (2012).
42. Yu, M.-F., Files, B. S., Arepalli, S. & Ruoff, R. S. Tensile loading of ropes of single wall carbon nanotubes and their mechanical properties. *Phys. Rev. Lett.* **84**, 5552–5555 (2000).
43. Bai, Y. et al. Carbon nanotube bundles with tensile strength over 80 GPa. *Nat. Nanotechnol.* **13**, 589–595 (2018).
44. Zhang, X. & Li, Q. Enhancement of friction between carbon nanotubes: an efficient strategy to strengthen fibers. *ACS Nano* **4**, 312–316 (2010).
45. Zhao, J. et al. Vibration damping of carbon nanotube assembly materials. *Adv. Eng. Mater.* **20**, 1700647 (2018).
46. Li, W. et al. Merge multiple carbon nanotube fibers into a robust yarn. *Carbon* **145**, 266–272 (2019).
47. Wang, J., Miao, M., Wang, Z., Humphries, W. & Gu, Q. A method of mobilizing and aligning carbon nanotubes and its use in gel spinning of composite fibres. *Carbon* **57**, 217–226 (2013).
48. Duan, Q. et al. Simultaneous improvement on strength, modulus, and elongation of carbon nanotube films functionalized by hyperbranched polymers. *ACS Appl. Mater. Interfaces* **11**, 36278–36285 (2019).
49. Liang, L. et al. Strong, healable, and recyclable composite paper made from a codispersion of carbon nanotube and sulfonated graphenal polymer. *Macromol. Mater. Eng.* **303**, 1800208 (2018).
50. Hong, L. & Liu, X. Sohu. Hammering irons to repair the bottom of pots. https://m.sohu.com/a/158734152_480185/ (2017).